Power Losses of Oil-Jet Lubricated Ball Bearings With Limited Applied Load: Part 2 - Experiments and Model Validation

F. de Cadier de Veauce, L. Darul, Yann Marchesse, T. Touret, Christophe Changenet, Fabrice Ville, L. Amar, C. Fossier

Tribology Transactions

ISSN: (Print) (Online) Journal homepage: https://www.tandfonline.com/loi/utrb20

Power Losses of Oil-Jet Lubricated Ball Bearings With Limited Applied Load: Part 2 - Experiments and Model Validation

F. de Cadier de Veauce, L. Darul, Y. Marchesse, T. Touret, C. Changenet, F. Ville, L. Amar & C. Fossier

To cite this article: F. de Cadier de Veauce, L. Darul, Y. Marchesse, T. Touret, C. Changenet, F. Ville, L. Amar & C. Fossier (2023): Power Losses of Oil-Jet Lubricated Ball Bearings With Limited Applied Load: Part 2 - Experiments and Model Validation, Tribology Transactions, DOI: 10.1080/10402004.2023.2235395

To link to this article: https://doi.org/10.1080/10402004.2023.2235395

Accepted author version posted online: 20 Jul 2023.

POWER LOSSES OF OIL-JET LUBRICATED BALL BEARINGS WITH LIMITED APPLIED LOAD: PART 2 - EXPERIMENTS AND MODEL VALIDATION

F. de Cadier de Veauce [a b c d], L. Darul [a b], Y. Marchesse [a], T. Touret [a], C. Changenet [a], F. Ville [b], L. Amar [c], C. Fossier [d]

[a] Univ Lyon, Ecam LaSalle, LabEcam, 69005 Lyon, France

[b] Univ Lyon, INSA Lyon, CNRS, LaMCoS, UMR 5259, 69621 Villeurbanne, France

[c] Cetim, 60300 Senlis, France

[d] NTN in Europe, 74010 Annecy, France

christophe.changenet@ecam.fr

ABSTRACT

This paper presents an experimental study on load independent power losses in oil jet lubricated deep groove ball bearings. These experiments were performed under different operating conditions. Rotational speed, lubricant temperature, oil flow rate and rolling element bearings dimensions were varied to quantify their influence on power losses. A load-independent power losses model for rolling element bearings has been proposed in a companion paper (Darul et al., 2023, "*Power Losses of Oil-Jet Ball Bearings with Limited Applied Load: Part 1 - Theoretical Analysis*") and was used here to simulate experiments. Model results and measurements are compared. A good agreement is found on the power losses in low loaded deep groove ball bearings.

KEYWORDS

Rolling Element Bearings, Power Losses, Experiments, Model, Test rig, Oil-jet Lubrication

INTRODUCTION

Energy consumption and associated power dissipation are growing concerns in transport and energy industries. Friction accounts for one-third of the energy used in transport, some of which comes from transmission [1]. Rolling element bearings (REBs) are widely used in the latter and can be a major source of power losses. This is even more true for electric vehicles, where rotational speeds become high and torque becomes low [2]. However the power losses at such speeds are still difficult to predict and further studies are needed. Losses in REBs are generally separated into two types: a) load dependent losses mainly due to sliding and friction between the rolling elements and the rings ; and b) load independent power losses [3] . The main load independent power losses are drag force, churning and lubricant shear due to the cage. This study focuses on theoretical and experimental investigations of load independent power losses in an oil jet lubricated REB.

Several studies have been published on these load independent power loss sources. Firstly, for drag and churning losses, respectively the force due to translation and rotation of moving parts in a fluid, numerous theoretical and numerical studies through CFD simulations have been published. They have helped to understand the lubrication mechanisms and to determine drag and churning losses in REBs [4-6]. SKF also developed a model for the calculation of drag and churning power losses [7]. Some analytical and experimental studies have also proposed a method for calculating churning losses of rotating cylinders in crossflow [8, 9]. A method to estimate drag power losses in REBs has been proposed, taking into account both the geometry of the REB and its thermal behavior [10]. Secondly, some experimental and analytical studies have

investigated lubrication of REB cage pocket [11]. These losses due to shearing of lubricant between the rolling elements and the cage can be calculated assuming Couette flow. These load independent power losses become significant at high rotational speeds but remain low at moderate speeds or less (rotational speed multiplied by REB mean diameter less than $1 \times 10^6\ mm.rpm$) [12].

Hydrodynamic rolling is another source of power losses that has been widely studied analytically for different lubrication regimes and systems[13-15]. As presented in literature, this source does not seem to be a part of load independent power losses because it depends on load [13]. For example, the SKF model for the calculation of rolling frictional moment uses REB geometry, speed, and load [16].

In a companion paper, Darul *et al.* [17] proposed a new model to predict the hydrodynamic rolling power losses in REB, caused by lubricant shearing at the contact inlet between rolling elements and rings [17]. In this model, hydrodynamic rolling power loss is calculated as the sum of losses both from loaded rolling elements considered in elasto-hydrodynamic lubrication (EHL) regime and the non-loaded rolling elements in isoviscous rigid (IVR) regime. While EHL rolling power losses are well known, the dissipative source from IVR regime is the purpose of the present investigation. This source is independent of the applied load. The major interest is that no parameter modification is required depending on the REB type used or its size for example, unlike other models such as Harris or SKF ones [16, 18]. This model is presented in the following and the results will be compared with experimental ones.

The hydrodynamic rolling model is first briefly introduced, more details being available in [17]. Then, the experimental study of oil jet lubricated deep groove ball bearings under low-load

conditions is presented, including test rig, the procedure, the two REBs tested, the test matrix and the measurements. The parametric study is performed with two different REBs, including oil jet temperature, oil flow rate and rotational speed. Then the influence of each parameter is discussed. The measurements and model simulations are then compared. Finally, a sensitivity study is made thanks to the model.

ROLLING POWER LOSS MODEL

One of the power loss sources in REBs is the hydrodynamic rolling, whatever the rotational speed is. It is due to the rise of pressure at the convergent inlet formed by the balls and the ring raceway, creating a dissymetry of the pressure field. Rolling power losses in REBs are usually modelled using elasto-hydrodynamic (EHD) theory and it can be calculated with Houpert [13] or Tevaarwerk [19] models. In the latter reference the hydrodynamic force that acts on the loaded balls is written as:

$$F_{HR_{EHD}} = Q_{n_j} \frac{a}{R_x} \left[4.25\, G^{*0.022}\, W^{*-0.87}\, U^{*0.66} \left(\frac{b}{a}\right)^{0.91} \right] \quad (1)$$

$F_{RH_{EHD}}$ is related to three dimensionless parameters U^*, G^* and W^* expressed as:

$$U^* = \frac{v_r\, \eta}{E'\, R_x} \;;\; G^* = \alpha_p\, E' \;;\; W^* = \frac{Q_{n_j}}{E'\, R_x^2} \quad (2)$$

Parameters a and b are respectively the semi-major and semi-minor dimensions of the Hertz ellipse. Rolling velocity v_r, equivalent Young modulus E' and equivalent radius in rolling direction R_x can be easily calculated knowing the materials properties and measuring the geometry of the REB raceway. Radial load distribution in REB can be estimated according to Harris [18]. Generally, some rolling elements are not loaded. Equation (1) cannot be used for unloaded rolling elements.

Darul *et al.* [17] proposed thus to consider isoviscous rigid (IVR) regime for unloaded rolling elements. In this case, the hydrodynamic rolling force in this regime becomes [13]:

$$F_{HR_{IVR}} = 0.835\left(\frac{R_x}{R_y}\right)^{-0.358} W^{*0.364}\,(2U^*)^{0.636}\,E'\,R_x^2 \quad (3)$$

The dimensionless load W^* is needed in equation (3) even though no load is applied on rolling elements. Darul *et al.* assume that the film thickness is equal to the clearance at the contact (in other words, equals to the REB diametral clearance P_d divided by four) to determine an equivalent load from film thickness in IVR regime and use it to calculate W^*[20]:

$$Q_{eq} = E'\,R_x^2\left[128\,R_x\,\frac{U^{*^2}}{\frac{P_d}{4}}\,\frac{\left(0.13\;atan\frac{1}{2\lambda}+1.68\right)^2}{\left(1+\frac{2\lambda}{3}\right)^2\lambda}\right]^{\frac{1}{2}} \quad (4)$$

Where P_d is the diametral clearance, and λ the equivalent radii ratio.

Finally, the rolling power losses can be calculated taking into account the loaded and unloaded contacts:

$$P_{HR} = \left(\sum_{loaded\ RE} F_{HR_{EHD}} + \sum_{unloaded} F_{HR_{IVR}}\right) v_r \quad (5)$$

This model is used in the present paper to evaluate rolling power losses. Sliding power loss is also calculated with SKF formula [16] and added to the model.

EXPERIMENTS ON LOAD-INDEPENDENT POWER LOSS IN ROLLING ELEMENT BEARING

Test Rig and Test Procedure

A REB test rig, originally developed by Niel *et al.* [21] and used by Brossier *et al.* [22] to study REB thermal behavior (Figure 1), has been used to measure REB power losses under different operating conditions. A detailed presentation is available in [21] and [22]. The test rig has been designed to test a wide variety of REBs. It is composed of a motor which operates a rotating shaft. This shaft is equipped with a torquemeter followed by two identical oil bath lubricated *support blocks* (in black on Figure 1). Same oil bath level is ensured in both blocks. Support blocks are sealed with lip seals. The tested REB is placed in a *measurement block* between the support blocks. The layout of the REB test rig is presented on Figure 2.

Limits and measurements performed during this test campaign. The highest rotational speed achieved is 9,700 rpm and radial load applied is 3 kN. Temperatures are measured with thermocouples on different parts of the test rig, including the outer rings of each REB and the inner ring of the measurement block with a telemetry device. Total torque is measured with the torquemeter placed on the shaft, between two elastic couplings. The signal is measured with strain gauges and the information is transmitted by induction. Other temperatures can be measured such as ambient air, block surface, oil bath, etc. When the measurement block is lubricated by injection, temperature of oil at nozzle inlet as well as injection and discharge oil flow rates are measured. Range and accuracy of sensors are summarized in Table 1.

Calibration. A calibration phase is necessary to isolate power losses of the tested REB from the total measured torque. The measurement block is replaced by a calibration block. This block has two oil bath-lubricated REBs and two lip seals, as in both support blocks. Two loads (1 kN and 3 kN) and 5 rotational speeds (from 3,200 to 9,700 rpm) are applied. Firstly, power loss contribution from radial lip seals has been measured.

Secondly, new series of tests with a complete calibration block were performed (with two seals and two REBs). This corresponds to a total of 6 seals and 4 REBs with support and calibration blocks. Thus, the power losses from support block REBs are expressed as a function of rotational speed, radial load and OR temperatures. Results from this function compared with losses of a support block REB are presented on Figure 3. Finally, by replacing the calibration block with the measurement one, it is possible to isolate tested REB losses from total torque measured on the test rig.

Rolling Element Bearings and Test Matrix

The two deep groove ball bearings (DGBB) shown in Figure 4 were tested in this study. The design parameters of these REBs and of those from the support blocks are provided in Table 2. Internal and detailed geometry is known for both tested REBs. Their osculation is known and defined by $f = r/D$, where r is the raceway groove curvature radius and D the ball diameter [18].

Some differences can be noticed, REB#1 has larger dimensions than REB#2. For example, the volume ratio $V_{\#1}/V_{\#2}$ is 2.9 with $V = \frac{\pi}{4}(d_o^2 - d_i^2)B$, and the ball diameter ratio is 1.6. Hydrodynamic losses are expected to be more important in REB#1 than in REB#2 due to curvature radii and ball diameters The experimental test matrix presented in Table 3 allows to study the influence of the following parameters.

Oil lubrication. Tests were performed with a gear box mineral oil. The physical properties of this oil are given in Table 4. The two REBs have been injection lubricated with a nozzle near to the REB, injecting at the centre of rolling elements. The lubricant temperature was regulated and heated up to 60°C. Some tests were also performed with an oil at ambient

temperature. Oil temperature is measured at the inlet of the injection nozzle. So, the impact of oil temperature and viscosity on power losses is studied within a range from 20°C ($\nu = 82.2\ cSt$) to 60°C ($\nu = 14.9\ cSt$).

Rotational speed. The rotational speed of each tested REB was fixed up to 9,700 rpm ($N.d_m$ of $0.848 \times 10^6\ mm.rpm$ and $0.679 \times 10^6\ mm.rpm$ for REB#1 and #2). The tests were either five-point tests with a rotational speed of 3,200 to 9,700 rpm and an increment of 1,600 rpm, or two-point tests at 3,200 and 9,700 rpm.

Load. As the interest lies in load independent power losses, the radial load applied on the tested REB is less than 10% of the static load C_0. Thus, for REBs #1 and #2 the radial loads applied are respectively 3,000 N and 1,000 N. No axial load is applied. As presented on Figure 5, there is no significant change in power losses between 0 N, 1,000 N and 3,000 N for support block REBs, showing that load independent power losses are well considered. The radial load applied on the tested REB has a slightly decrease during the tests and is compensated to get back to the initial value.

Flow rate. The oil flow rate values are defined for each test. Two oil flow rates are tested for REB#1 at 15 and 35 L/h, and two other ones for REB#2 at 6 and 15 L/h. In addition, at the bottom of the blocks, on each side of the REB, discharge pipes are used to avoid oil bath in the blocks.

Power Loss Measurement Results

Figure 6 illustrates the evolution of REB#1 torque with time during the experiment for different values of rotational speed and oil injected temperature. Torque values can be close from each other and thus are difficult to interpret. Moreover, power losses values seem more relevant for

analysis purpose as heat exchange and thermal behavior of the system are considered here [21]. Since tests do not start always at the same initial temperatures, it seems more relevant to plot the torque or the power loss according to ring temperatures instead of time. Moreover, high temperatures are achieved in a shorter time at high speed than at low speed, while experimental results are in the same range of outer ring temperature. As depicted, temperatures and power losses does not always reach stationary regime, especially at higher speed. Tests are stopped when IR temperature is equal or greater than 100°C to avoid cage deformations and too much thermal expansion.

Figure 7 shows the evolution of measured power losses versus OR temperature for REB #1 considering different values of oil injected temperature (25 and 60°C), and speeds (3,200 and 9,700 rpm). Oil flow rate and radial load are fixed at 35 L/h and 3 kN. Losses decrease with increasing OR temperature whatever the operational conditions, due to the decrease of the oil mist viscosity in the REB. Rotational speed seems to influence power losses while there is no change with the injected oil temperature. Same trends are observed for REB#2 at 3200 rpm and 8070 rpm (Figure 8). This observation is in line with Dowson and Higginson [14] who point out that the controlling factor is the viscosity of the oil at the ring bulk temperature and that the temperature of the oil supply has little influence.

A comparison is provided Figure 9 for different oil flow rates, with REB #1. Radial load do not change and oil injection temperature is fixed at 60°C. A slight power loss increase at equivalent OR temperature is noticed from 15 to 35 L/h (Mean relative difference around 11% at 3,200 rpm, and 17% at 9,700 rpm). It seems that oil flow rate does not have a great influence either. The same trends are observed for REB #2 with oil flow rate from 6 to 15 L/h (Figure 10) (Mean relative difference is 6.2% at 3,200 rpm and 14.7% at 8,070 rpm). The results are similar to those

of [23] with oil flow rate from 39 to 78 L/h (Figure 11) (At 65°C, relative difference is 14.9% at 3,100 rpm, 4.8% at 8,070 rpm and 8.4% at 10,000 rpm). The slight rise in power losses with increasing oil flow rate can be explained by a larger amount of oil in the REB and thus more drag losses [10, 22, 24].

Figure 12 compares the measured power losses of REB #1 for different speed values (from 3,200 to 9,700 rpm). The oil flow rate, radial load, injected oil temperature are kept constant and equal to 35 L/h, 3 kN and 60°C respectively. As previously explained, power losses increase with rotational speed, but decrease with temperature. This result is in agreement with global models such as Harris or SKF ones.

The comparison of the power losses generated by REBs #1 and #2 is given in Figure 13 for two different speeds, (3,200 rpm and 8,070 rpm). Oil flow rate equals 15 L/h for both REBs. The average power loss ratio $P_{\#1}/P_{\#2}$ is varying between 2.07 and 2.81 for the five speeds tested, keeping the same configuration for each tests. The average power loss ratio for all speeds is 2.45. Since the only change is the bearing size, with REB#1 larger than REB#2, the REB size may have an impact on power loss values. This will be discussed in more detail in the next section.

COMPARISON OF THE MODEL WITH EXPERIMENTS

Experiments are compared to the above mentioned model [17] in the "Rolling Power Loss Model" section, and to the global model developed by Harris and Palmgren [18], the resistive torque being recalled:

$$M_0 = 10^{-10} \times (\nu\, N)^{2/3}\, f_0\, d_m^3 \qquad (6)$$

$$M_1 = f_1\, F_r\, d_m \qquad (7)$$

$$f_1 = z\left(\frac{F_r}{C_0}\right)^y \qquad (8)$$

Where M_0 and M_1 are respectively the load independent and load dependent contributions. The value for the parameter f_0 is 4 for oil jet lubricated deep groove ball bearings from Harris [18], but it is set to 2 from previous studies [21]. The latter one is considered in this study. The parameter f_1 can be calculated and its value is 4.5×10^{-5} for REB#1 and 3.6×10^{-5} for REB#2 in the present study. The power loss due to oil shearing between rolling elements and the cage is neglected, especially at high speed [11]. Also, as rotational speeds are moderate ($N.d_m < 1 \times 10^6\ mm.rpm$), drag and churning losses are neglected. The mean temperature between the measured outer and inner ring is used in the models to calculate oil viscosity. Load dependent power losses due to sliding are calculated with SKF model and added to the hydrodynamic rolling power loss [16]. The following figures present REB measured power losses and model results according to the OR temperature. All relative differences are presented in Table 5 and Table 6, with ε_{exp} and ε_{Harris} respectively the mean relative errors with experiments and with Harris model.

In Figure 14(a), comparisons between experiment and model power losses for REB#1 are presented at five different speeds. Oil flow rate and injection temperature are kept constant at 35 L/h and 60°C respectively. Both models estimate that power losses decrease with OR temperature and increase with rotational speed. Better results are obtained at higher temperatures with the models. For OR temperature close to 30 or 40°C, large differences can be observed up to 270 W at 9,700 rpm while good agreements at less than 100 W are observed at low speed (from 3,200 to 6,400 rpm). In Figure 14(b), the power losses of REB#2 are presented

at five different speeds when oil flow rate and temperature are equal to 15 L/h and 60°C respectively. Good agreements are found at low and high speeds, with an average relative error of 12.0 %.

As it has been said previously, f_0 value is given in tables from Harris depending on both the type of lubrication and the type of REB. However, previous studies found this value should be modified in order to predict power losses [22]. In the present study, f_0 needs to be determined for each REB to have the best fitting between experimental results and Harris model. The two following values have been found: 1.65 and 1.40 for REB#1 and #2 respectively. These values are used with the Harris' model in the following. Developed model results are really close to Harris' results with an average relative difference of 6.6 %.

According to the experimental results presented earlier, the average power losses ratio between REB#1 and #2 is equal to 2.45. This result can be compared with the theoretical power loss ratio $M_{0,\#1}/M_{0,\#2}$ obtained with Harris model:

$$\frac{M_{0,\#1}}{M_{0,\#2}} = \frac{f_{0,\#1}}{f_{0,\#2}} \times \left(\frac{d_{m,\#1}}{d_{m,\#2}}\right)^3 = \frac{1.65}{1.40} \times \left(\frac{87.5}{70}\right)^3 = 2.30 \quad (9)$$

This result is close to the ratio obtained with experiments, relative difference is equal to 6.1% when taking into account two different f_0 while it is equal to 20.3% if the same f_0 is considered. The parameter f_0 must therefore be modified according to the REB geometry and size. Similar experimental work has been done by Brossier [22], comparing two REBs of different dimensions but with the same operating conditions. Once more the f_0 value must be adjusted to REB dimension.

Figure 15 is a comparison between the experimental losses, the simulated losses with rolling EHL and IVR models and sliding, and the losses calculated from Harris, for five speeds. Calculations are in good agreement with measurements. Sliding contribution fits well with M_1, Harris load-dependent torque, but is not sufficient to explain experimental power losses. Rolling EHL and IVR contributions can explain M_0, the load-independent torque of Harris [18]. This latter source represents an important part of measured power losses, the IVR cannot be neglected, and this is valid for both REBs.

Figure 16(a) shows the measured and calculated power losses of REB#1 at 3,200 and 9,700 rpm and with an oil flow rate at 35 L/h for ambient oil injection (near 25°C). The experimental results are well predicted, the maximum absolute error being less than 48 W at 3,200 rpm and 140 W at 9,700 rpm. The model always gives results close to those of Harris, the average relative error being less than 8.3 % (see Table). Figure 16(b) presents results for REB#2 with an oil injected at ambient temperature, for three different speeds. Mean relative errors are less than 8.4 % with the model compared to experiment and less than 5.8 % compared to Harris one.

The comparison between measured and predicted values is satisfactory for a wide range of rotational speed. The proposed developed model shows good agreements with Harris model, as can be seen in Table 5 and Table 6. There is no need to adjust any parameter, unlike to the different f_0 values for each REB with Harris model.

A strong assumption is made on the oil film thickness in IVR regime, which was assumed to be equal to the clearance at the contact. A sensitivity study is carried out on the REB#1 diametral clearance, which was measured and initially $34\ \mu m$. The model is tested for a diametral clearance of $10\ \mu m$, $2\ \mu m$, and $0.1\ \mu m$ keeping the same assumption on the oil film thickness. Figure 17 shows power losses of REB#1 calculated with the model for the four different assumptions and experimental losses, for a rotational speed of 6,400 rpm, an oil flow rate of 35 L/h and injected oil at 60°C. A decrease in REB clearance can be due to thermal expansion as the temperature of the REB parts increases.

As observed on Figure 17(a), power losses increase as REB clearance decreases. The same trend is noticed at each speed. It is more relevant to focus on high ring temperatures due to thermal expansion as on Figure 17(b). Better results are obtained with the known and used clearance value of $34\ \mu m$. The power losses increased on average by 7.9% ± 1.2% from $34\mu m$ to $10\mu m$. They increased by 18.5% ± 2.9% for $2\mu m$, and of 47.5% ± 8.0% for $0.1\mu m$. The initial assumption seems to be the best choice and in good agreement with experimental results. Moreover, REB clearance does not induce a big difference in power losses if the value remains close to the initial value.

CONCLUSIONS

An experimental study on load independent power losses in oil jet lubricated REBs has been presented in this paper. The experiments were designed in order to show the influence of speed, oil flow rate, oil jet temperature, speed and REB geometry on load-independent power losses. The experimental results were compared with a developed model [17] to predict power losses due to hydrodynamic rolling. Results from the proposed model provided predictions that correlated well with measurements over a range of operating conditions such as rotational speed, oil properties and REB geometry, with an average relative error of 11.8 %. The model was also compared with the widely used power losses global model from Harris and Palmgren. The two models showed good agreement despite the fact that Harris uses a fixed parameter according to the REB tested.The proposed model only considers geometry and oil properties for any REB but it requires knowledge of the internal geometry of the REB.

Although the model predicts the experiments well, it can still be improved. In this study, the measured OR and IR temperatures were used to calculate the power losses because it is difficult to measure the temperature of other parts, such as rolling elements and oil inside the REB. Nevertheless, these temperatures can be estimated using a thermal network, discretising REB in several isothermal nodes, connected by thermal resistances, as performed for REB in previous works[10, 12, 22]. A combined model with power losses and thermal aspects provides better accuracy and more information. Furthermore, this work is only based on jet lubrication, further studies are required for oil bath lubrication.

ACKNOWLEDGMENTS

The authors are grateful to Association Nationale de la Recherche et de la Technologie (ANRT)

(CIFRE No. 2020/1522).

REFERENCES

[1] Holmberg, K., and Erdemir, A. (2019), "The impact of tribology on energy use and CO2 emission globally and in combustion engine and electric cars," Tribology International, **135**, pp 389-396.

[2] Neurouth, A., Changenet, C., Ville, F., Velex, P., Octrue, M. (2014), “Is splash lubrication compatible with efficient gear units for high-speed applications?” in International Gear Conference, Lyon, France, pp 1060-1068.

[3] Palmgren, A. (1967), "Les Roulements: Description, Théorie, Applications," 2nd edition, SKF.

[4] Gao, W., Nelias, D., Boisson, N., and Lyu, Y. (2018), "Model formulation of churning losses in cylindrical roller bearings based on numerical simulation," Tribology International, **121**, pp 420-434.

[5] Marchesse, Y., Changenet, C., and Ville, F. (2014), "Numerical Investigations on Drag Coefficient of Balls in Rolling Element Bearing," Tribology Transactions, **57**, pp 778-785.

[6] Peterson, W., Russel, T., Sadeghi, F., Tekletsion Berhan, M., Stacke, L.-E., and Stahl, J. (2021), "A CFD investigation of lubricant flow in deep groove ball bearings," Tribology International, **154**, pp 1-15.

[7] Morales-Espejel, G., and Wemekamp, A. (2022), “An engineering drag losses model for rolling bearings,” Proceedings of the Institution of Mechanical Engineers, Part J: Journal of Engineering Tribology, pp 1-16.

[8] Aldoss, T., and Abou-Arab, T. (1990), "Experimental Study of the Flow Around a Rotating Cylinder in Crossflow," Experimental Thermal and Fluid Science, **3**, pp 316-322.

[9] Rumbarger, J., Filetti, E., and Gubernick, D. (1973), "Gas Turbine Engine lainshaft Roller Bearing-System Analysis," Journal of Lubrication Technology, pp 401-416.

[10] Pouly, F., Changenet, C., Ville, F., Velex, P., and Damiens, B. (2010), "Power Loss Predictions in High-Speed Rolling Element Bearings Using Thermal Networks," Tribology Transaction, **53**(6), pp 957-967.

[11] Russell, T., and Sadeghi, F. (2022), "The effects of lubricant starvation on ball bearing cage pocket friction," Tribology International, **173**, pp 1-14.

[12] Niel, D., Changenet, C., Ville, F., and Octrue, M., (2019), "Thermomecanical study of high speed rolling element bearing: A simplified approach," Proceedings of the Institution of Mechanical Engineers, Part J: Journal of Engineering Tribology, **233(**4), pp 541-552.

[13] Biboulet, N., and Houpert, L. (2010), “Hydrodynamic force and moment in pure rolling lubricated contacts. Part 2: point contacts,” Proceedings of the Institution of Mechanical Engineers, Part J: Journal of Engineering Tribology, **214**, pp 777-787.

[14] Dowson, D., and Higginson, G. (1977), “Elasto-Hydrodynamic Lubrication,” SI Edition, Pergamon Press Ltd., Oxford, UK, ISBN 0 08 021303 0.

[15] Houpert, L. (1987), “Piezoviscous-Rigid Rolling and Sliding Traction Forces, Application: The Rolling Element-Cage Pocket Contact,” Journal of Tribology, **109**, pp 363-370.

[16] SKF Group (2013), Rolling Bearings Catalog.

[17] Darul, L., Touret, T., Changenet, C. and Ville F. (2023), " Power Losses of Oil-Jet Lubricated Ball Bearings with Limited Applied Load: Part 1 - Theoretical Analysis," Tribology Transactions.

[18] Harris, T. A. (1991), “Rolling Bearing Analysis,” third Edition, John Wiley and Sons Inc., New York, USA, ISBN 0 471 51349 0.

[19] Tevaarwerk, J. L., and Johnson, K. L. (1979), “The Influence of Fluid Rheology on the Performance of Traction Drives,” ASME Transactions Journal of lubrication technology, **101**, pp 266-274.

[20] Brewe, D., and Hamrock, B. (1982), "Analysis of Starvation Effects on Hydrodynamic Lubrication in Nonconforming Contacts," Journal of Lubrication Technology, **104**(3), pp 410-417.

[21] Niel, D., Changenet, C., Ville, F., and Octrue, M. (2018), “A new test rig to study rolling element bearing thermomechanical behavior,” in International Gear Conference, Lyon, France, pp 121-133.

[22] Brossier, P., Niel, D., Changenet, C., Ville, F., and Belmonte, J. (2020), “Experimental and numerical investigations on rolling element bearing thermal behaviour,” Proceedings of the Institution of Mechanical Engineers, Part J: Journal of Engineering Tribology, pp 1-12.

[23] Giannetti, G., Meli, E., Rindi, A., Ridolfi, A., Shi, Z., Tangredi, A., Facchini, B., Fondelli, T., and Massini, D. (2019), "Modeling and experimental study of power losses in a rolling bearing," Proceedings of the Institution of Mechanical Engineers, Part J: Journal of Engineering Tribology, pp 1-20.

[24] Parker, R. J. (1984), "Comparison of Predicted and Experimental Thermal Performance of Angular-Contact Ball Bearings," NASA Technical Paper, **2275**, pp 1-16.

NOMENCLATURE

List of Symbols

a, b	Dimensions of the contact ellipse, m
B	Bearing width, m
C_0	Static load, N
D	Rolling element diameter, m
d_i	Inner ring diameter, m
d_m	Mean diameter, m
d_o	Outer ring diameter, m
E'	Equivalent Young modulus = $2/[(1-\nu_1^2)/E_1 + (1-\nu_2^2)/E_2]$, Pa
f	Osculation = r/D, -
f_0, f_1	Harris parameters
F_{HR}	Hydrodynamic rolling force, N
F_r	Radial load, N
G^*	Dimensionless materials parameter = $\alpha\ E'$, -
M_0, M_1	Load independent and dependent torques, N.m
N	Rotational speed, rpm
P_d	Diametral clearance, m
P_{HR}	Hydrodynamic rolling power loss, W
Q	Radial load on rolling elements, N

Q_{eq}	Equivalent load for IVR regime, N
r	Raceway groove curvature radius, m
R_x, R_y	Equivalent radii, m
U^*	Dimensionless speed = $v_r\ \eta/E'R_x$, -
v_r	Rolling velocity, m/s
W^*	Dimensionless load = $Q/E'R_x^2$, -
Z	Number of rolling elements, -
α_p	Pressure-viscosity coefficient, Pa^{-1}
ε	Mean relative error, -
η	Dynamic viscosity, Pa.s
λ	Radii ratio = R_x/R_y, -
ν	Kinematic viscosity, mm^2/s (cSt)

TABLES AND FIGURES

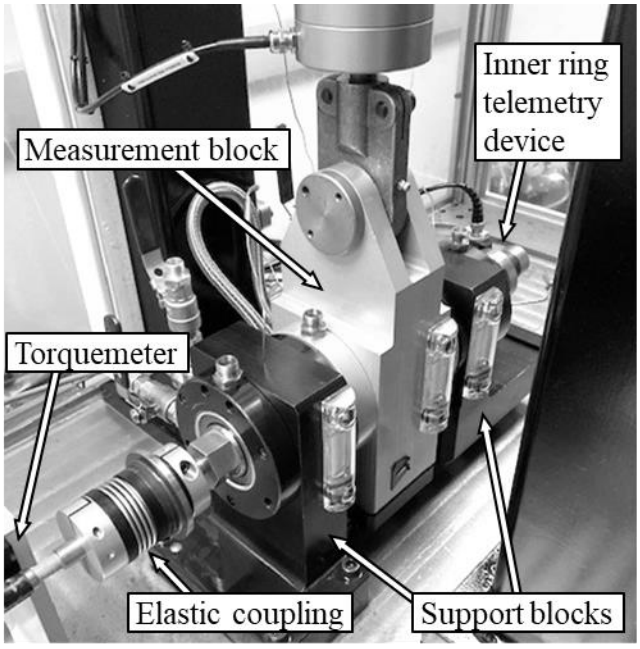

Figure 1 View of the REB test rig, from the left to the right: the torquemeter, an elastic coupling, the first support block, a measurement block and the second support block.

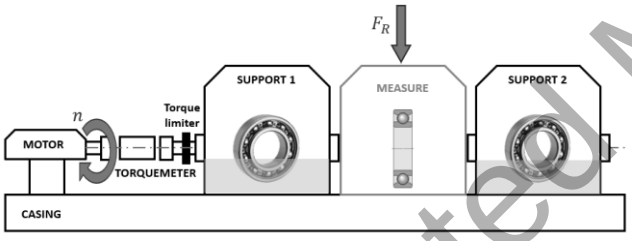

Figure 2 Scheme of the REB test rig

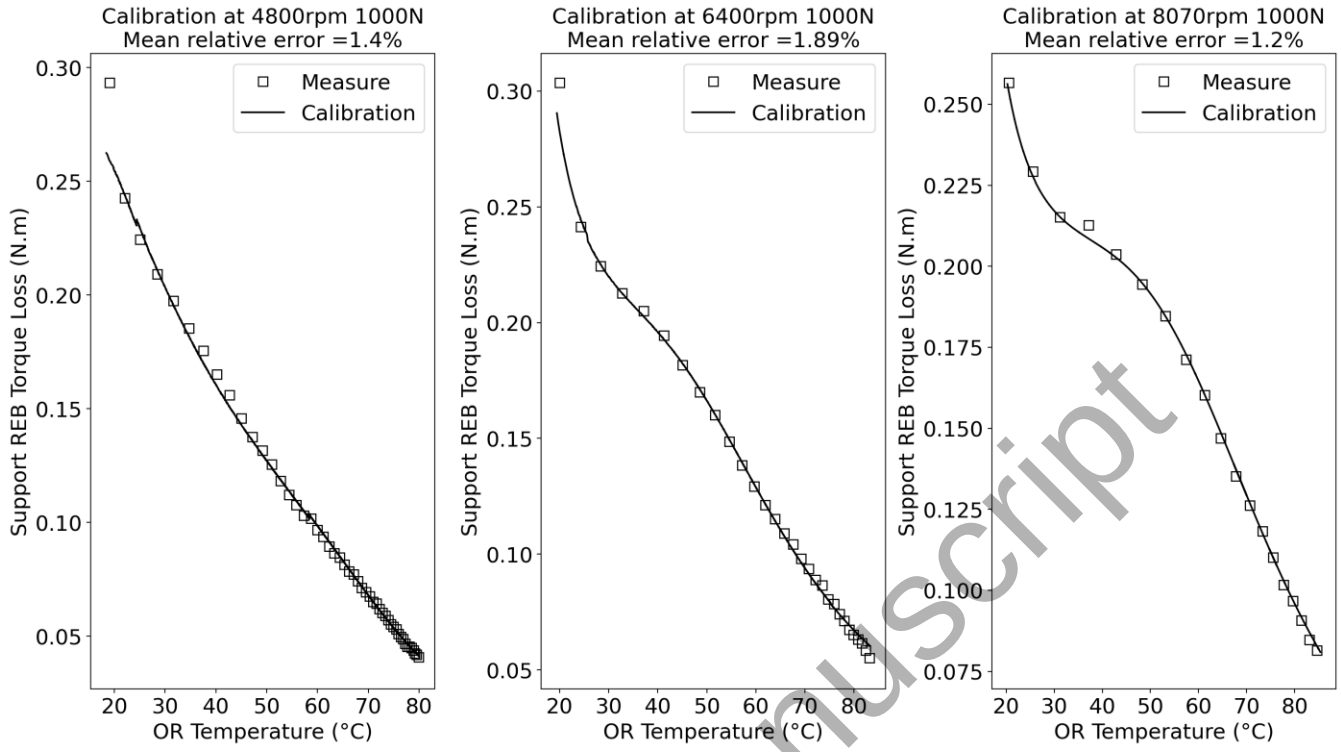

Figure 3 Calibration results for a support block REB at 4,800 rpm, 6,400 rpm, and 8,070 rpm and 1 kN applied.

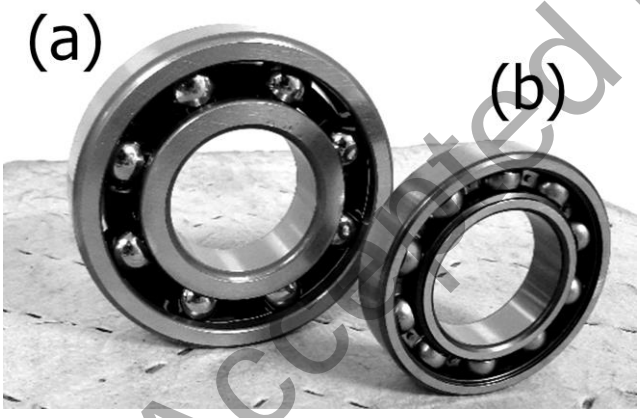

Figure 4 **(a)** REB #1 with $d_m = 89$ mm **(b)** REB #2 with $d_m = 70$ mm

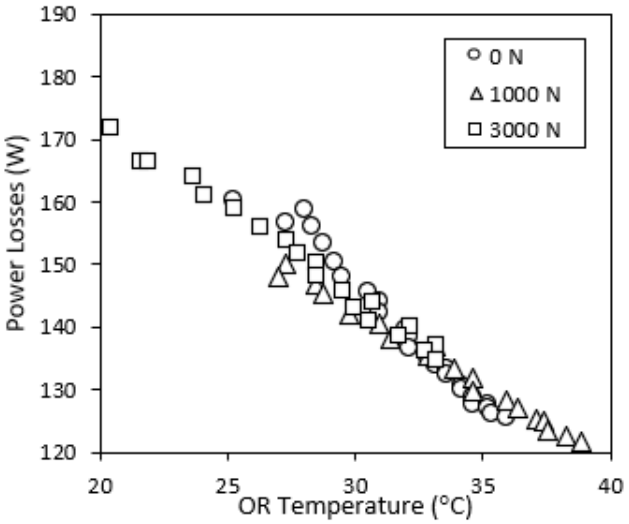

Figure 5 Power losses versus the outer ring temperature of the support block REBs for three radial loads (0 N, 1200 N and 3000 N), at 4800 rpm.

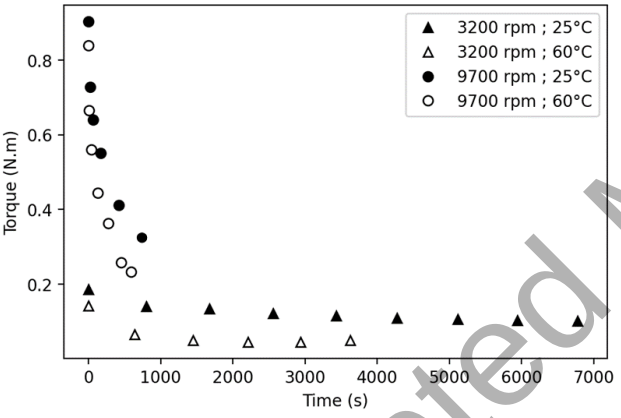

Figure 6 Measured torque versus time, after calibration.

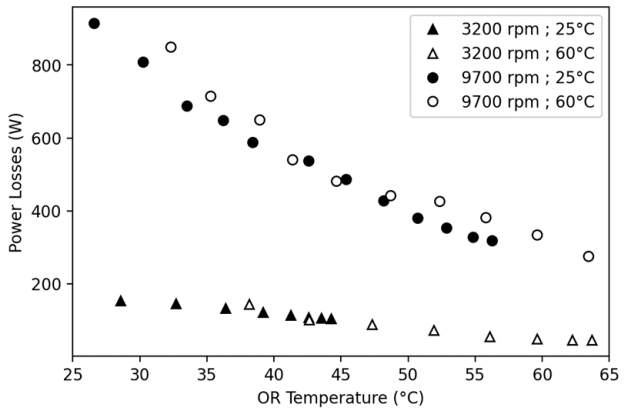

Figure 7 Power losses versus outer ring temperature of the REB #1 for two speeds (3200 and 9700 rpm) and for two oil injection temperatures (25 and 60°C), oil flow rates equals 35 L/h and radial load is 3 kN.

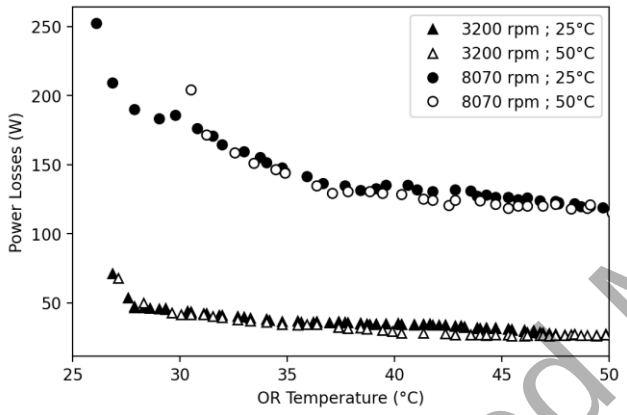

Figure 8 Power losses versus the outer ring temperature of the REB #2 for two speeds (3200 and 8070 rpm) and for two oil injection temperatures (25 and 50°C) , oil flow rate equals 15 L/h and radial load is 1 kN.

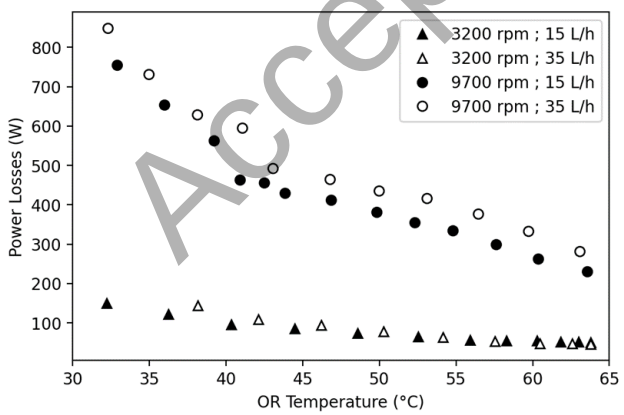

Figure 9 Power losses versus the outer ring temperature of the REB #1 for two speeds (3,200 rpm and 9,700 rpm) and for two oil flow rates (15 L/h and 35 L/h), with oil at 60°C

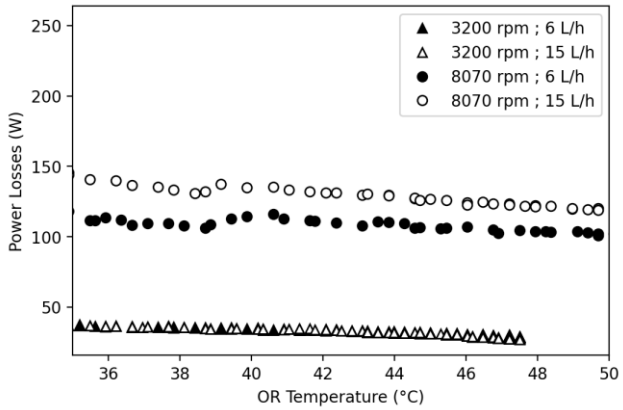

Figure 10 Power losses versus the outer ring temperature of the REB #2 for two speeds (3200 and 8070 rpm) and for two oil flow rates (6 and 15 L/h), with oil at 25°C

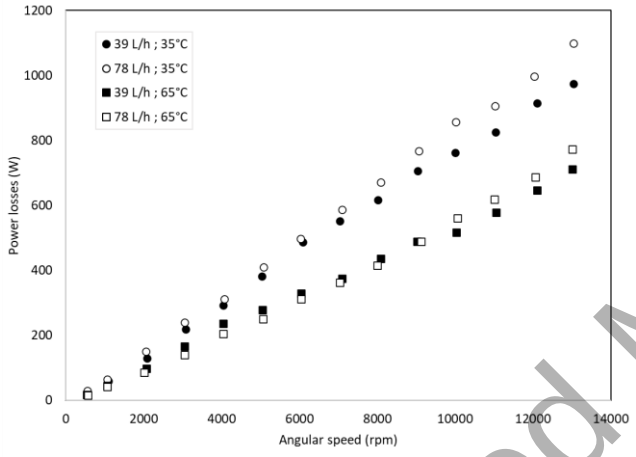

Figure 3 Power losses versus the rotational speed, results from [21], with oil flow rate and lubricant initial temperature

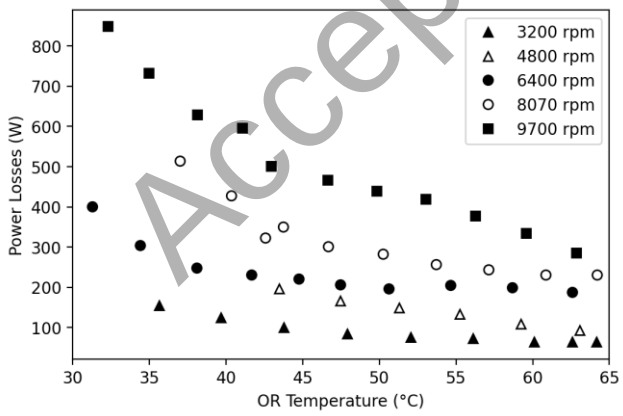

Figure 4 Power losses versus the outer ring temperature of the REB #1 with oil at 60°C and an oil flow rate at 35 L/h.

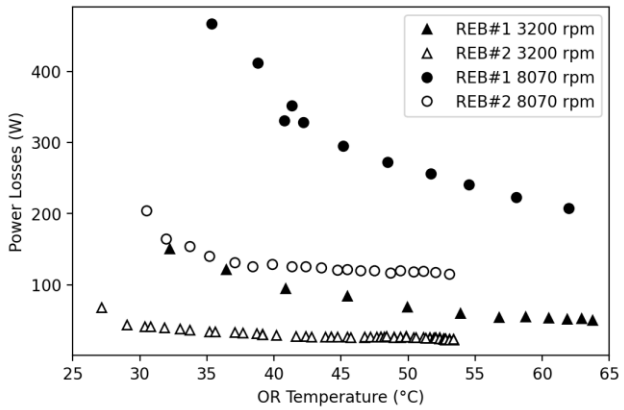

Figure 5 Power losses versus outer ring temperature for the two REBs at 3200 and 8070 rpm.

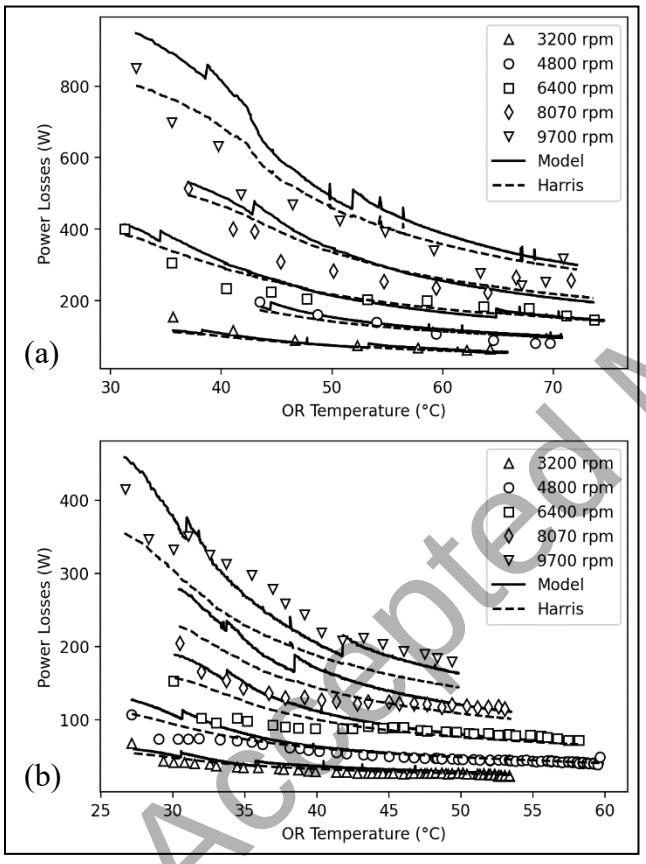

Figure 6 Power losses at several speeds compared with the developed model and with Harris model. Oil temperature at 60°C. REB#1 with oil flow rate at 35 L/h (a) REB#2 with oil flow rate at 15 L/h (b).

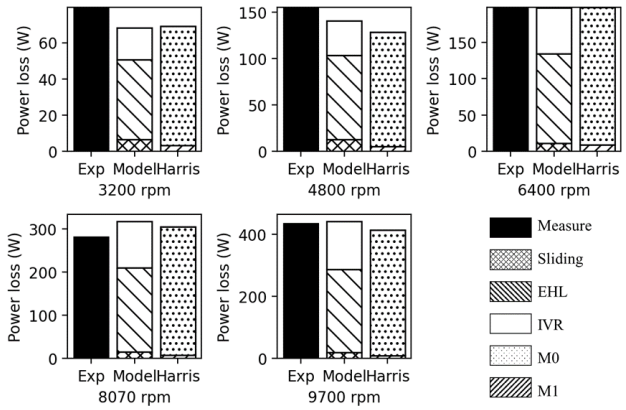

Figure 7 Power losses distribution of REB #1 when OR temperature equals 50°C for five different speeds.

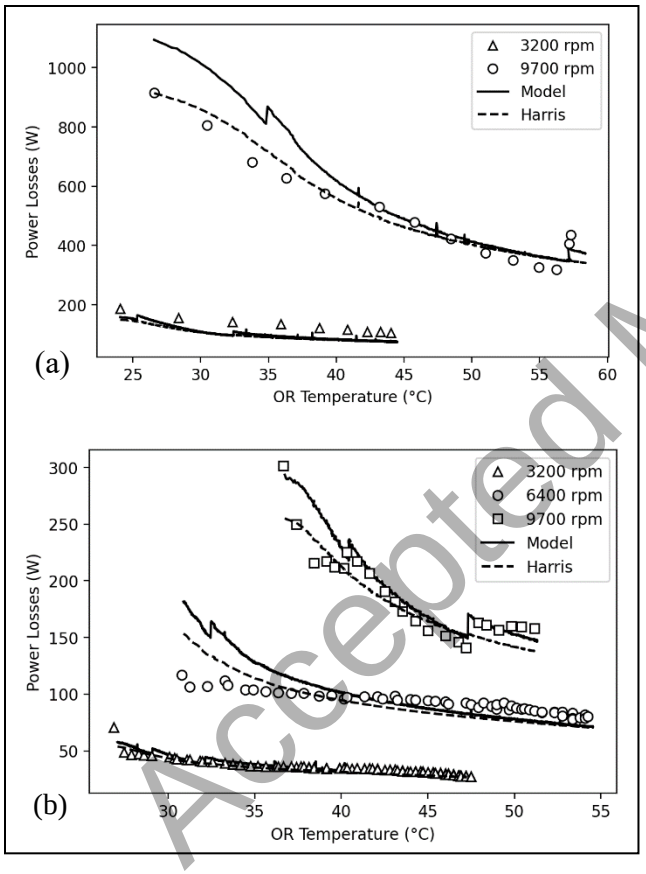

Figure 8 Power losses for REB#1 with oil temperature at 25°C and flow rate at 35 L/h (a) REB#2 with oil temperature at 25°C and flow rate at 15 L/h (b).

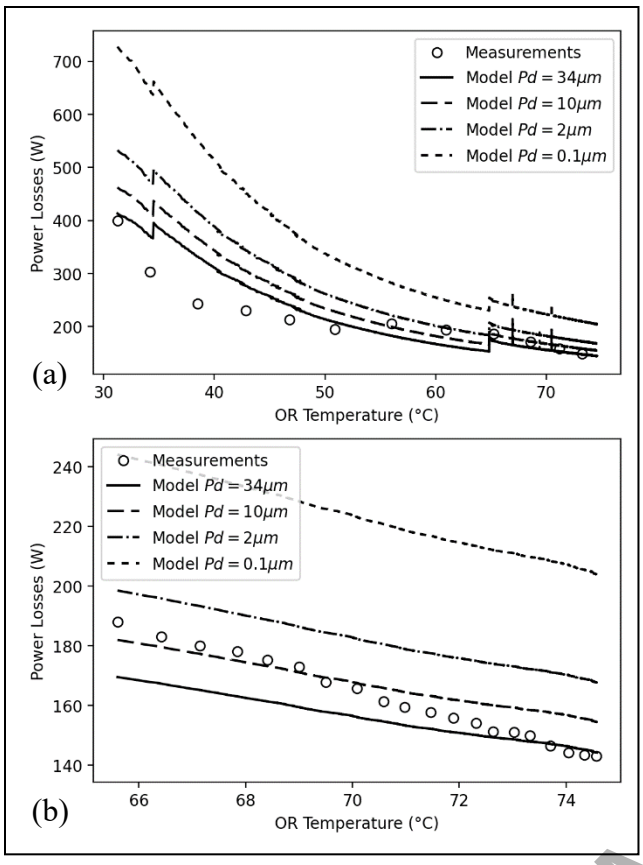

Figure 9 Sensitivity study on REB #1 diametral clearance at 6400 rpm, 35 L/h, 60°C (a) focus at high temperature (b).

Sensors	Range	Accuracy
Torquemeter	0 to 10 N.m	0.02 %
Thermocouple	-40 to +125 °C	0.5 °C
Force sensor	0 to 20 kN	0.4 %
Flow sensor	15 to 550 l/h	1.0 %

Table 1 Instrumentation characteristics

Parameter	Support REB	Tested REB #1	Tested REB #2
Bore diameter d_i (mm)	50	55	50
Outer diameter d_o (mm)	72	120	90
Mean diameter d_m (mm)	61	87.5	70
Width B (mm)	12	29	20
Static load C_0 (kN)	11.8	45.0	23.2
Number of balls Z	16	8	10
Ball diameter D (mm)	6.7	20.6	12.7
Inner osculation		0.51	
Outer osculation		0.52	

Table 2 REB Characteristics

Test n°	REB ref.	Speed (rpm)	Oil temp. (°C)	Flow rate (L/h)
1	#1	Five-point (3200 to 9700)	60°C	15
2	#1	Five-point (3200 to 9700)	60°C	35
3	#1	Two-point (3200 to 9700)	25°C	35
4	#2	Five-point (3200 to 9700)	25°C	6
5	#2	Five-point (3200 to 9700)	25°C	15
6	#2	Five-point (3200 to 9700)	50°C	15

Table 3 Experimental test matrix

Kinematic viscosity at 40°C (cSt)	36.6
Kinematic viscosity at 100°C (cSt)	7.8
Density at 15°C ($kg.m^{-3}$)	864.6

Table 4 Oil properties

Speed	ε_{exp}	ε_{Harris}
3200 at 60°C	7.4 %	7.0 %
4800 at 60°C	9.4 %	6.4 %
6400 at 60°C	7.4 %	4.0 %
8070 at 60°C	15.5 %	3.3 %
9700 at 60°C	16.2 %	11.4 %
3200 at 25°C	27.6 %	5.7 %
9700 at 25°C	8.8 %	8.3 %

Table 5 Relative differences between model results and experiments or Harris global model for REB#1

Speed	ε_{exp}	ε_{Harris}
3200 at 60°C	15.3 %	7.8 %
4800 at 60°C	5.8 %	2.7 %
6400 at 60°C	15.1 %	8.2 %
8070 at 60°C	16.1 %	15.0 %
9700 at 60°C	7.5 %	17.8 %
3200 at 25°C	5.1 %	3.4 %
6400 at 25°C	12.8 %	6.1 %
9700 at 25°C	7.3 %	8.0 %

Table 6 Relative errors between model results and experiments or Harris global model for REB#2